PAPER • **OPEN ACCESS**

Thermal mapping analysis of a 48V prismatic lithium-ion battery pack with active and passive cooling

To cite this article: Antonio Paolo Carlucci *et al* 2023 *J. Phys.: Conf. Ser.* **2648** 012098

Thermal mapping analysis of a 48V prismatic lithium-ion battery pack with active and passive cooling

Antonio Paolo Carlucci, Hossein Darvish, and Domenico Laforgia

Department of Engineering for Innovation, University of Salento, via per Monteroni, 73100, Lecce, Italy

paolo.carlucci@unisalento.it,
hossein.darvish@unisalento.it,
domenico.laforgia@unisalento.it

Abstract. This experimental study investigates the thermal behavior of a 48V lithium-ion battery (LIB) pack comprising three identical modules, each containing 12 prismatic LIB cells, during five charge-discharge cycles. A homogeneous liquid cooling system is applied at the bottom of the modules to control the pack temperature when it reaches 40°C (active cooling phase). The initial two cycles represent passive cooling, where the cooling liquid remains stationary. Temperature distribution is measured and analyzed using 27 thermocouples, providing insights into temperature changes in the cells, modules, pack, and cooling system inlet/outlet. Results show that in passive cooling cycles, minimum temperature occurs at pack surfaces due to better convective heat transfer, while maximum temperature is observed in the central LIB cells. The active cooling phase alters the temperature distribution within the pack. One module is found to be more sensitive to high currents, generating more heat and releasing it faster. Additionally, the positive tab temperature is higher than the negative tab temperature within a single cell. The liquid cooling system decreases the temperature rise from 5.8°C to 3.5°C in the discharge cycles with a constant current of -237A. This study emphasizes the significance of evaluating the thermal behavior of individual modules and highlights the complexity of the LIB pack system, as well as the impact of an indirect liquid cooling system on enhancing its thermal performance.

1. Introduction

Electric Vehicles (EVs) have emerged as a viable solution to address the issue of Carbon Dioxide (CO_2) emissions in the atmosphere. They offer benefits such as reduced pollution levels, lower noise, smoother operation, and regenerative braking [1]. There are approximately 20 million passenger EVs on the road as of mid-2022 [2]. However, this number is expected to increase significantly, with a projected 77 million passenger EVs on the road by 2025. These vehicles will constitute 6% of the global fleet, 13% in China, and 8% in Europe [2]. Despite the short-term setbacks caused by the coronavirus pandemic during 2019-2022, the long-term outlook for EVs remains undiminished [2].

Hybrid Electric Vehicles (HEVs) combine the efficiency of EVs with the range capabilities of conventional vehicles [3]. Forecasts have predicted that HEVs will capture 36% of the market share by 2030 [4]. HEVs can be categorized into micro, mild, and full HEVs based on the increasing levels of electrical system voltage [5]. Among them, the 48V Mild Hybrid Electric Vehicle (MHEV) provides a

promising solution for reducing both cost and CO_2 emissions [6,7]. Therefore, the present study focuses on a 48V battery pack with the application of MHEVs.

For MHEVs, rechargeable Lithium-Ion Batteries (LIBs) are considered an appropriate energy storage solution due to their high energy density, specific power, and lightweight. Compared to other rechargeable batteries like lead-acid, nickel-cadmium, and nickel-metal hydride batteries, LIBs exhibit lower self-discharge rates, higher recyclability, and longer life cycles [8–10]. Moreover, the price of LIB packs has significantly declined over the past 13 years, dropping nearly 90% from over $1000 per kW/h in 2010 to $151 per kW/h at the end of 2022 [11,12].

Previous research has highlighted the primary challenges of LIBs, including high temperature and uneven temperature distribution. For instance, LIB cells experienced a substantial loss of initial power at elevated temperatures, with more than 60% loss at 50.0°C after 800 cycles and 70% loss at 55.0°C after 500 cycles [13]. Temperature also influences the cycle life of LIB cells, with a significant drop in cycles from 3323 at 45.0°C to 1037 at 60.0°C [14]. Therefore, temperature plays a critical role in determining the life cycle and energy capacity of LIB cells.

To address these temperature-related challenges, a Battery Thermal Management System (BTMS) is essential for maintaining proper battery temperature and minimizing temperature variations between cells [15,16]. BTMSs can be classified based on power consumption, heat transfer medium, and contact between the coolant and battery surface. Conventional techniques for battery cooling include air cooling, liquid cooling, and phase change materials cooling [17–19].

Air cooling, classified as free and forced convection cooling, is a cost-effective method used in earlier versions of EVs such as the Volkswagen EV race car and Nissan Leaf [17–19]. It offers advantages such as simplicity, low cost, electrical safety, lightweight design, ease of maintenance, and no leakage concerns.

Liquid cooling systems, on the other hand, provide superior thermal performance and cooling efficiency compared to air cooling due to a higher thermal conductivity and specific heat capacity of liquids. This technique for battery cooling can be used directly, also called dielectric liquid, or indirectly in contact with the coolant and battery surface (indirect liquid cooling system). This commercialized technique is used in liquid-cooled EVs such as the Chevrolet Volt, Tesla Model S and Model 3, BMW i3, and i8 [17–19]. In this study, we consider an indirect liquid cooling system.

Existing research on LIBs has primarily focused on individual cells or packs with a limited number of thermocouples to monitor thermal behavior [6,7,20–25]. For instance, cell studies have investigated thermal uniformity, the influence of charging and discharging rates, and the effect of cell sizes on temperature distribution [20,21]. However, these studies lack a comprehensive analysis of external parameters, like the presence of other cells, on LIB cell behavior. There is also a limited scope of research on the thermal behavior of 48V LIB packs. While some pack studies have examined the overall temperature, voltage, and current of a battery pack during driving cycles, they did not explore temperature distribution across individual cells within the pack [6,22]. Consequently, there is a gap in understanding the detailed temperature distribution of a complete LIB pack in automotive applications.

To address these gaps, this study focuses on a LIB pack employing an indirect liquid cooling system. The thermal performance of the pack is experimentally investigated through five full charge-discharge cycles, utilizing 25 thermocouples positioned at various locations within the pack. The extensive use of sensors in this study provides valuable insights into the thermal behavior of the battery pack, which is a novel approach not previously reported in the literature to the best of the authors' knowledge. Additionally, two temperature sensors are employed to monitor the cooling liquid temperature at the inlet and outlet of the pack. With respect to our previous work [26], in which the temperature distribution of a 48V LIB pack during two fully charge-discharge cycles was examined, this paper introduces a notable advancement. The effectiveness of an indirect liquid cooling system in managing the temperature of the LIB pack when it exceeds the desired maximum threshold is investigated in the present study.

Table 1. Main characteristics of the LIB cells and pack used in this study.

Parameter	Cell value	Pack value
Shape type (-)	Prismatic	12s3p
Chemistry (-)	NCM	NCM
Nominal capacity (Ah)	8.23	24.69
Nominal voltage (V)	3.7	44.4
Maximum voltage (V)	4.17	50
Maximum current (A)	233	700
Dimensions – length×width×height (mm)	144×17×60	660×475×132

The rest of this work is organized as follows: section *materials and methods* provides an overview of the experimental setup, LIB cell and pack parameters, the indirect liquid cooling system, notations, and the theoretical background. Section *results and discussion* presents the findings of the experimental tests and their discussion, including temperature measurements, average temperature, and temperature differences between battery cells, modules, and the pack, as well as inlet and outlet temperatures of the liquid cooling system. Finally, section *conclusion* summarizes the conclusions drawn from this study and future research is provided in this section as well.

2. Materials and methods

2.1. Lithium-ion battery cell parameters

LIB cells consist of positive and negative electrodes, electrolytes, separators, and current collectors. In the automotive industry, cylindrical, prismatic, and pouch shaped batteries are commonly employed [27,28]. Among them, prismatic shaped batteries are preferred due to their increased space utilization and flexibility. Thus, prismatic shaped LIBs are utilized in this study.

In the EV battery industry, the use of Lithium Nickel Manganese Cobalt Oxide (NCM) batteries, $LiNiMnCoO_2$, is on the rise [11,29]. NCM batteries offer advantages such as high C-rate capability during charge and discharge, long lifespan, and good performance at low temperatures [30]. Therefore, NCM LIB cells are considered in this study. Each LIB cell has a nominal voltage and capacity of 3.7V and 8.23Ah, respectively. Table 1 presents the geometrical and electrical parameters of the LIB cells used in this study.

2.2. Lithium-ion battery pack parameters

The thermal performance of a 48V LIB pack, which includes a cooling system, with the application on an MHEV is investigated in this study. The choice of a 48V LIB pack is based on its ease of installation in an MHEV, minimal impact on the overall weight, safe and compact modular design, and cost-effective performance in terms of fuel efficiency. The battery pack consists of multiple individual cells connected in series and parallel configurations to increase voltage and capacity, respectively. The LIB pack utilized in this study aligns with previous works by the same authors [26,31]. A 12s3p configuration is used, meaning that three cells are connected in parallel, and 12 sets of these three parallel cells are connected in series. Table 1 provides the properties of the battery pack used in this study, and Figure 1a illustrates the structure of the pack, modules, and cells. The LIB cells are separated by thin thermal barriers. In the original pack, there are various wirings, a Battery Management System (BMS) circuit, electrical devices such as shunt and relay, and an aluminum chassis which have not been reproduced as they are complex both from a structural point of view and from that of the materials used. The whole components are surrounded by a metal sheet as its dimensions are reported in Table 1 as well.

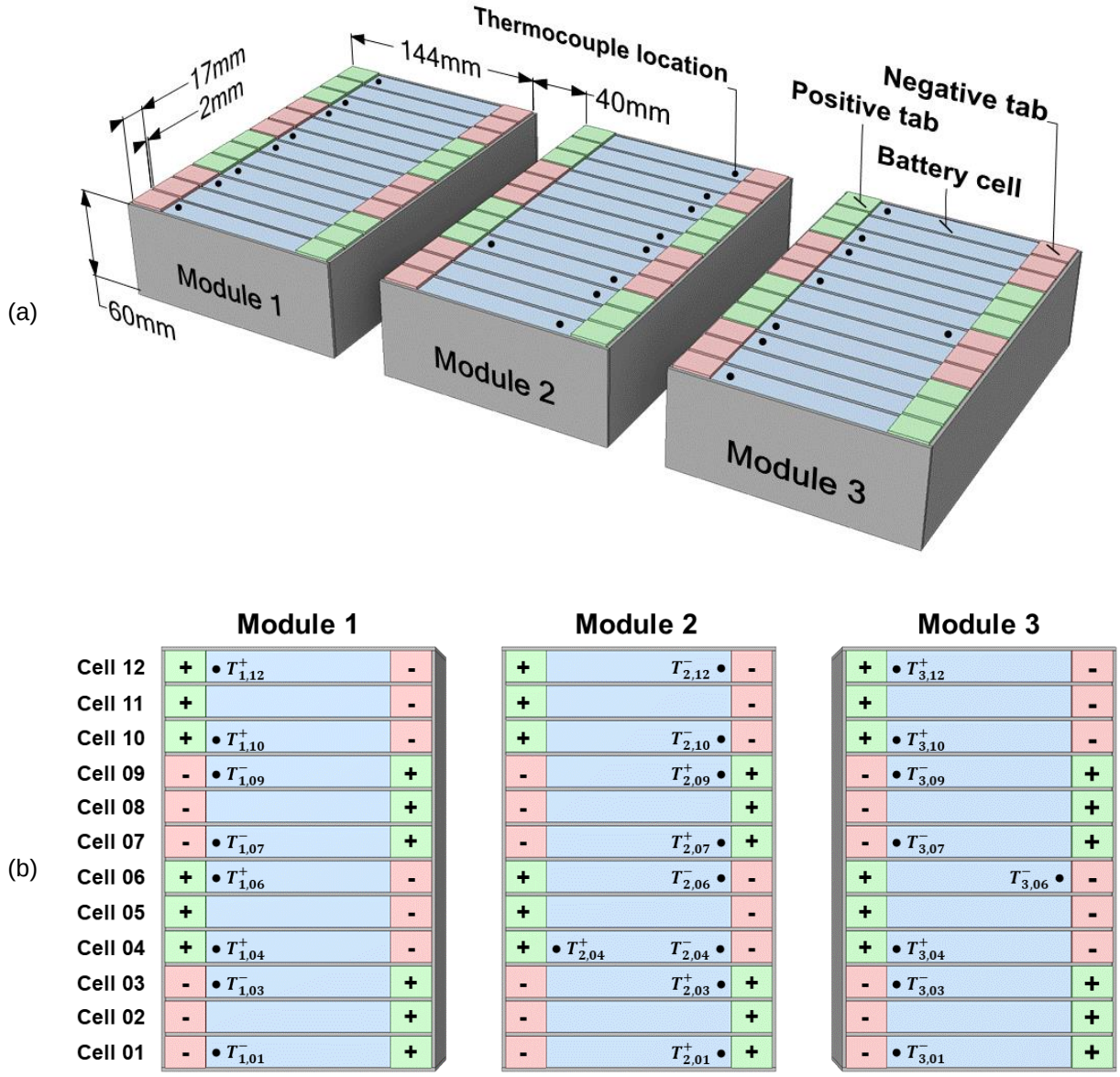

Figure 1. a) A trimetric view of the battery pack showing the connections and dimensions of the cells and the positions of the thermocouples. b) A top view of the model showing thermocouple positions and names in Module1, Module2, and Module3.

A homogeneous indirect liquid cooling system is employed at the bottom of the three modules when the pack temperature reaches approximately 40.0°C. They are connected through two inlet and outlet tubes to transfer the liquid to the channels. The liquid cooling used in this study is a mixture of water and ethylene glycol. The cooling system can be divided into two distinct phases based on its operation. Firstly, during the passive cooling phase, the cooling system is filled with the liquid; therefore, it remains stationary without any circulation. Secondary, when the liquid within the cooling system circulates (when the temperature threshold is reached), resulting in an active cooling system.

2.3. Experimental setup

Figure 2 depicts the experimental test setup utilized in this study, consisting of five main parts:

- a battery pack including a BMS,

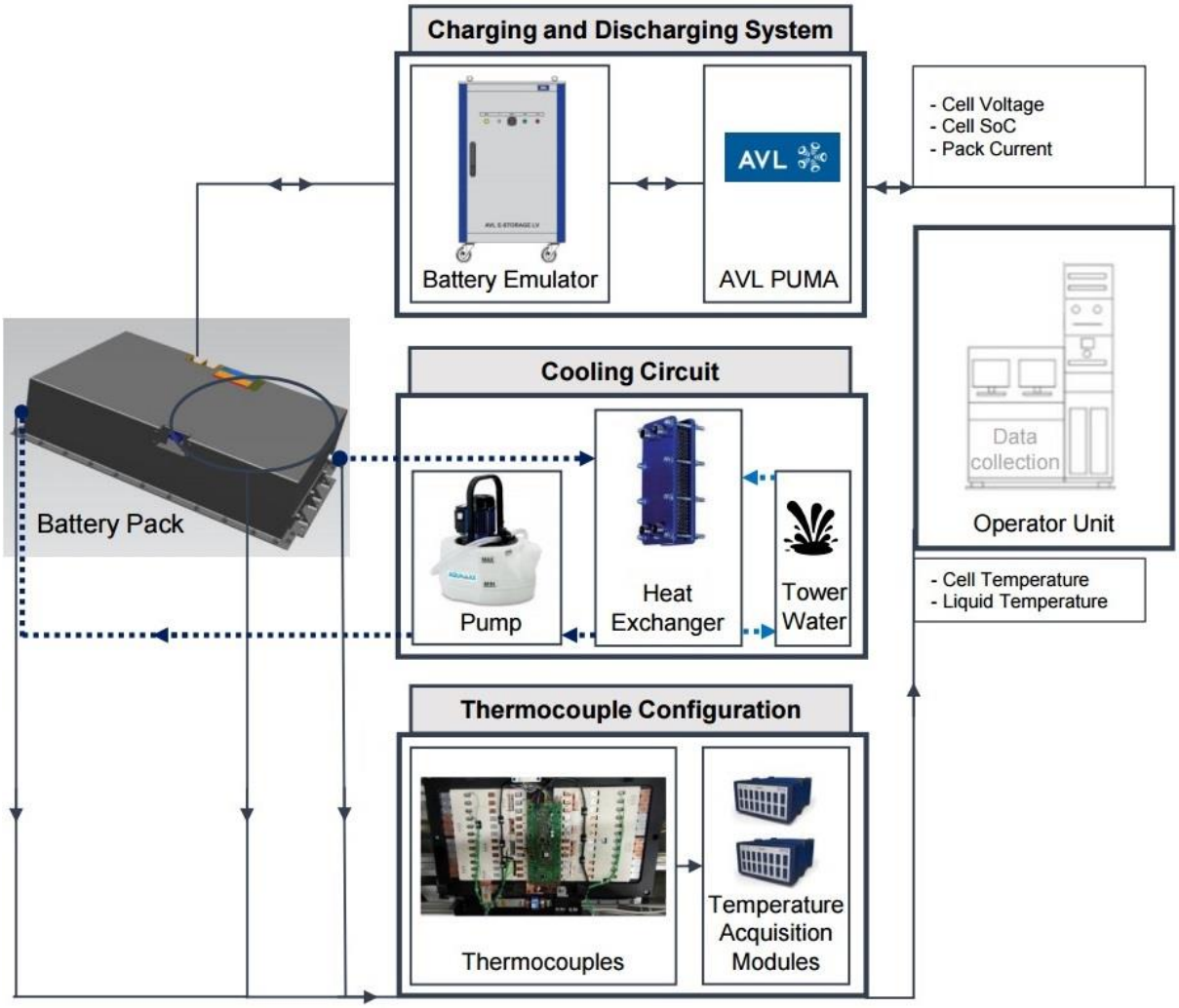

Figure 2. A schematic of the LIB pack thermal performance and cooling system setup.

- a high voltage - high current AVL battery emulator controlled by AVL PUMA system,
- 27 K-type temperature sensors with two data acquisition modules (ES620 ETAS),
- a liquid circuit for the cooling system comprising a water pump and a heat exchanger, and
- a computer unit for monitoring and storing data.

Among the 27 thermocouples, 25 ones are used to measure the temperature of the LIB cells, as illustrated in Figure 1. The thermocouples are positioned in three modules of the battery pack referred to as Module1, Module2, and Module3, as shown in Figure 1b. The naming convention for the measurement points is defined in *Theoretical background* section.

The highest temperature in LIB cells occurs near the tabs [23,24,32]. The tabs refer to the thin metal strips that are attached to the electrodes within the battery cell allowing the flow of the electrons between the electrodes and the external circuit. Thus, in this study, $T^{+}_{2,04}$ and $T^{-}_{2,04}$ are positioned in close proximity to the positive and negative tabs of the same cell (Figure 1b). In addition, the two remaining thermocouples as labeled by $T_{l,i}$ and $T_{l,o}$, measure the temperature of the inlet liquid cooling to the battery pack and the outlet one, respectively.

The experimental campaign aimed at analyzing the thermal performance of the battery pack was conducted at the "Center for Studies of Vehicle Components S.p.A" in Bosch plant in Modugno 70026, Bari, Italy.

2.4. Charging and discharging cycles

Five full charge-discharge cycle tests have been conducted in this experiment, starting at an initial temperature and State of Charge (SOC) of 26.2°C and 47%, respectively. The maximum and minimum currents recorded during the cycles are 237A and −237A, respectively, while the SOC ranges from 10% to 91%. The test concludes when the SOC reaches its maximum value at the fifth cycle. These cycles help to monitor the thermal behavior of the battery pack under different SOC values during both charging and discharging.

2.5. Theoretical background

The temperature effects on batteries are mainly related to internal materials and chemical reactions occurring within them. Heat generation within LIB cells (Q_{gen}) is associated with charge transfer and chemical reactions during charging and discharging [30,33]. The heat generated taking place in LIB cells, Equation 1, can be divided into reversible (Q_{rev}) and irreversible (Q_{irr}) processes [32,34–36].

$$Q_{gen} = Q_{irr} + Q_{rev} \tag{1}$$

The reversible heat originates from the reversible entropy change during electrochemical reactions (Equation 2), while the irreversible heat is caused by various processes such as active polarization, ohmic heating, and enthalpy change (Equation 3) [33,37–39].

$$Q_{rev} = -I \cdot T \cdot \frac{\partial U_{OCV}}{\partial T} \tag{2}$$

$$Q_{irr} = I \cdot (U_{OCV} - V_t) \tag{3}$$

where I is the terminal current (A), whose sign is positive when discharged, T is the temperature in the battery (°C), U_{OCV} is the open circuit voltage (V), and V_t is the terminal voltage. Q_{irr} becomes zero when the current reaches zero; therefore, the heat of mixing is not considered.

According to the laws of thermodynamics, the transient behavior of the heat generated inside the LIB cells results in different temperatures over time and distance. Thus, the resulting temperature on different LIB cells represents the heat generation of a complex system.

To analyze the thermal behavior of the LIB cells and pack, specific temperature positions are identified and named according to their module, cell, and tab position (Figure 1b), as illustrated in Equation 4:

$$T_{i=1,\dots,25}(t) = T^{z}_{m,c}(t) \tag{4}$$

where m presents the module number (1, 2, or 3), c indicates the cell number and assumes one value in the range of 01 to 12, as each module contains 12 cells, and the superscript z, either - or +, represents the negative or positive tab, respectively.

The maximum and minimum temperatures ($T_{max}(t)$ and $T_{min}(t)$) are defined as the highest and lowest temperature reached in the battery module or pack at each time between the measured temperature using thermocouples. The temperature difference ($\Delta T(t)$) is calculated as the difference between $T_{max}(t)$ and $T_{min}(t)$. T_{rise} is the difference between the initial and final temperature in a specific period. The temperature average ($T_{avg}(t)$) is calculated as the average temperature over a specific number of temperature points.

Furthermore, to study the thermal performance of the cooling system, the temperature difference ($\Delta T_l(t)$) is calculated as the difference between the temperature of the inlet and outlet ($T_{l,i}(t)$ and $T_{l,o}(t)$) liquid at each time.

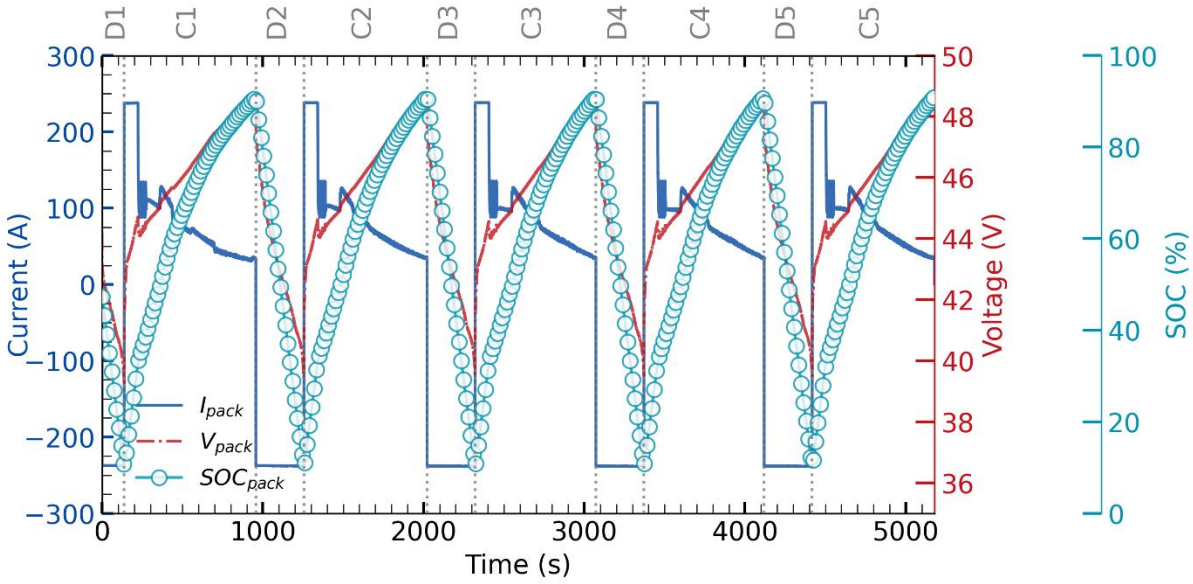

Figure 3. The dynamic changes in current, SOC, and voltage of LIB pack.

3. Results and discussion

3.1. State of charge and voltage

Figure 3 provides a comprehensive visualization of the voltage, current, and SOC of the battery pack. The applied current ranges from -237A to 237A, representing the minimum and maximum values, respectively. To facilitate a detailed analysis of the results, the test duration has been divided into two sections for each of the five cycles, namely the discharge period (D) and the charge period (C). The numerical indicators from 1 to 5 have been assigned to each abbreviation, corresponding to cycles 1 to 5, respectively.

In the initial section of the first cycle (D1), the current is maintained at -237A for 140s to transition the SOC from 47% to 10%. During this period, both the pack voltage and cell voltage decrease from 44.16V and 3.68V to 39.24V and 3.27V, respectively (assuming the cell voltage is estimated as 1/12 of the pack voltage).

Moving to the second section of the first cycle (C1), the current remains constant at 237A until 226.5s, resulting in an SOC of 33% and an increase in pack voltage to 44.71V (high current charging portion). Subsequently, the current decreases to 33A, leading to an SOC of 91% and a battery pack voltage rise to 48.68V. The second cycle starts at 959.5s (D2). Throughout the remaining cycles (D2 and C2 to D5 and C5), the pack current, SOC, and voltage exhibit temporal evolution similar to that described for D1 and C1. The only difference lies in the discharge periods (Ds) since, unlike the first cycle, they initiate at the maximum value of the SOC. The test finishes at 5180s.

While in the literature of studying LIB cells, it is common to consider only battery limitations in terms of SOC, it is worth noting that LIB pack applications in the real world often require high constant currents for extended periods of time. Consequently, the BMS reduces the output well below the maximum static limit to ensure safety and prevent damage. Figure 3 illustrates this trend, with a constant current of 237A, where the limit drops suddenly during the last part of each charging portion. The decrease in battery limits is due to battery thermal management elaborations to protect the battery.

3.2. Thermal performance

3.2.1. Cell stud y

As mentioned previously, the first portion of the test is named passive cooling, which is shown with a white background in Figures 4 and 5. In addition, the second portion of the test with the presence of the liquid cooling system is named active cooling, that is depicted by the blue portion in Figures 4 and 5.

The temperature time histories of the 25 thermocouples positioned in Module1, Module2, and Module3 are depicted in Figure 4. In the passive cooling portion, $T^{+}_{1,12}$ and $T^{-}_{2,12}$ represent the $\mathrm{T_{min}(t)}$ for Module1 and Module2, respectively. $T^{+}_{3,12}$ corresponds to the second lowest temperature value observed in Module3. However, in the third and fourth cycles, these values, relative to other points within the same module, increase, and in the final cycle (cycle 5th), they represent the $\mathrm{T_{max}(t)}$ for the respective module (active cooling portion).

Furthermore, during the passive cooling portion, the $\mathrm{T_{max}(t)}$ is observed in the middle cells; in particular, in Module1, $\mathrm{T_{max}(t)}$ is recorded in $T^{-}_{1,03}$, $T^{+}_{1,04}$, and $T^{+}_{1,06}$. In Module2, $\mathrm{T_{max}(t)}$ occurs in $T^{+}_{2,04}$ and $T^{+}_{2,07}$. Module3 exhibits $\mathrm{T_{max}(t)}$ in three internal cells: $T^{+}_{3,04}$, $T^{-}_{3,06}$, and $T^{-}_{3,07}$. However, in the subsequent cycles (active cooling portion), all of these highest temperatures shift towards the middle or lowest temperature points within each module.

The transition between $\mathrm{T_{max}(t)}$ and $\mathrm{T_{min}(t)}$ between passive and active cooling portions, can be attributed to two factors. Firstly, in the absence of flowing liquid during the first two cycles, the main heat transfer occurs to the air. Consequently, due to convective heat transfer from the boundary cells to the ambient environment, cells located on the surfaces of the pack exhibit the lowest temperatures, while the middle cells experience the highest temperatures during the initial cycles. Moreover, in cycles with the active cooling system (depicted by the blue portion in Figure 4), the heat transfer to the liquid medium becomes more influential compared to air. As the middle cells tend to have higher temperatures, the temperature difference between these cells and the liquid medium is greater, resulting in higher energy transfer between the middle cells and the liquid medium.

Furthermore, it is worth noting that $\mathrm{T_{min}(t)}$ of Module3 consistently occurs in $T^{-}_{3,01}$ across all cycles (Figure 4c). This observation emphasizes the complexity of this dynamic system and underscores the significance of evaluating the temperature behavior of a substantial number of battery cells within a battery pack during the research phase.

Finally, the temperature time histories of thermocouples positioned close to the negative and positive tabs on the same LIB cell are captured by $T^{-}_{2,04}$ and $T^{+}_{2,04}$, respectively. It is observed that the positive tab temperature ($T^{+}_{2,04}$) is higher than the negative tab temperature ($T^{-}_{2,04}$), which aligns with findings reported in the literature [23,24,32,34]. The maximum temperature difference between them is approximately 0.6°C.

3.2.2. Module study

Figure 4a illustrates the temperature behavior of Module1 during each cycle. The $\mathrm{T_{max}(t)}$ of Module1 at each cycle happens in the charging periods (C1 to C5). In C2 to C5, the maximum temperatures occur at the beginning of the corresponding charging cycles, reaching values of 40.2°C, 44.1°C, 45.8°C, and 45.3°C. These points correspond to the times when the high current charging of 237A concludes. In C1, unlike the other charging periods, two maximum temperature points are observed (approximately 32.7°C), with the second one occurring in the middle of that time section. The evolution of $\mathrm{T_{max}(t)}$ in Module2 and Module3 in the five cycles shows a similar pattern to that described for Module1 in C1 to C5 (Figures 4b and 4c). Finally, the highest temperature values for Module1, Module2, and Module3 throughout the entire test are observed at the beginning of C4, measuring 45.8°C, 45.0°C, and 44.6°C, respectively.

In Figure 5 the time histories of T_{avg}, T_{max}, T_{min}, and ΔT are presented for the entire battery pack as well as for each module. The T_{avg} of Module2 and Module3 exhibits a similar trend as the T_{avg} of the LIB pack. However, the T_{avg} of Module1 is slightly higher than that of the pack in discharge periods and at the beginning of the charging periods (when high currents of 237A are involved, either in charging or discharging). This observation shows that Module1 is more sensitive to high currents and thus generates more heat compared to the other modules.

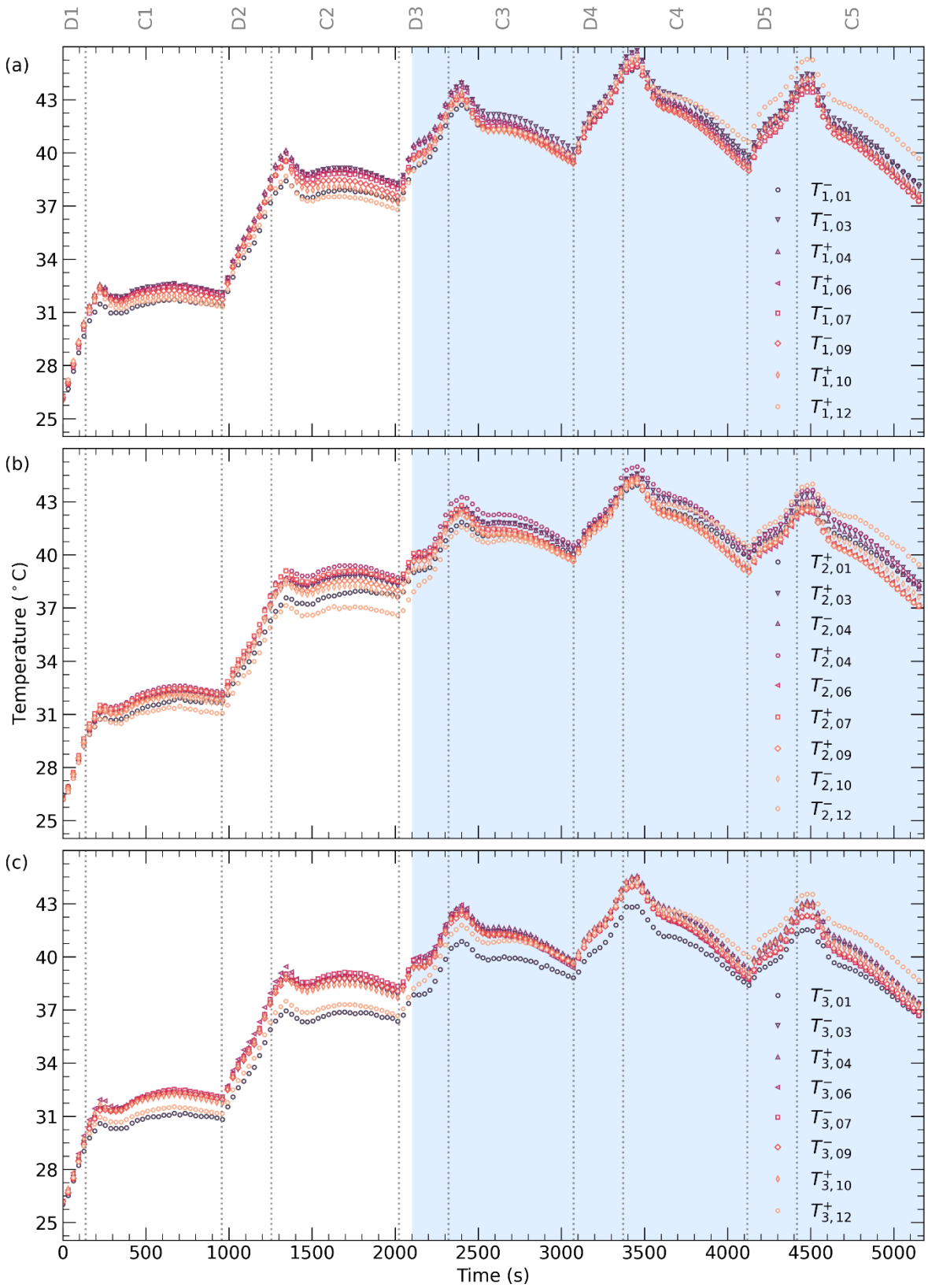

Figure 4. Temperature time histories of the thermocouples placed in a) Module1, b) Module2, and c) Module3. In all plots, the light blue area depicts the active cooling portion of the test.

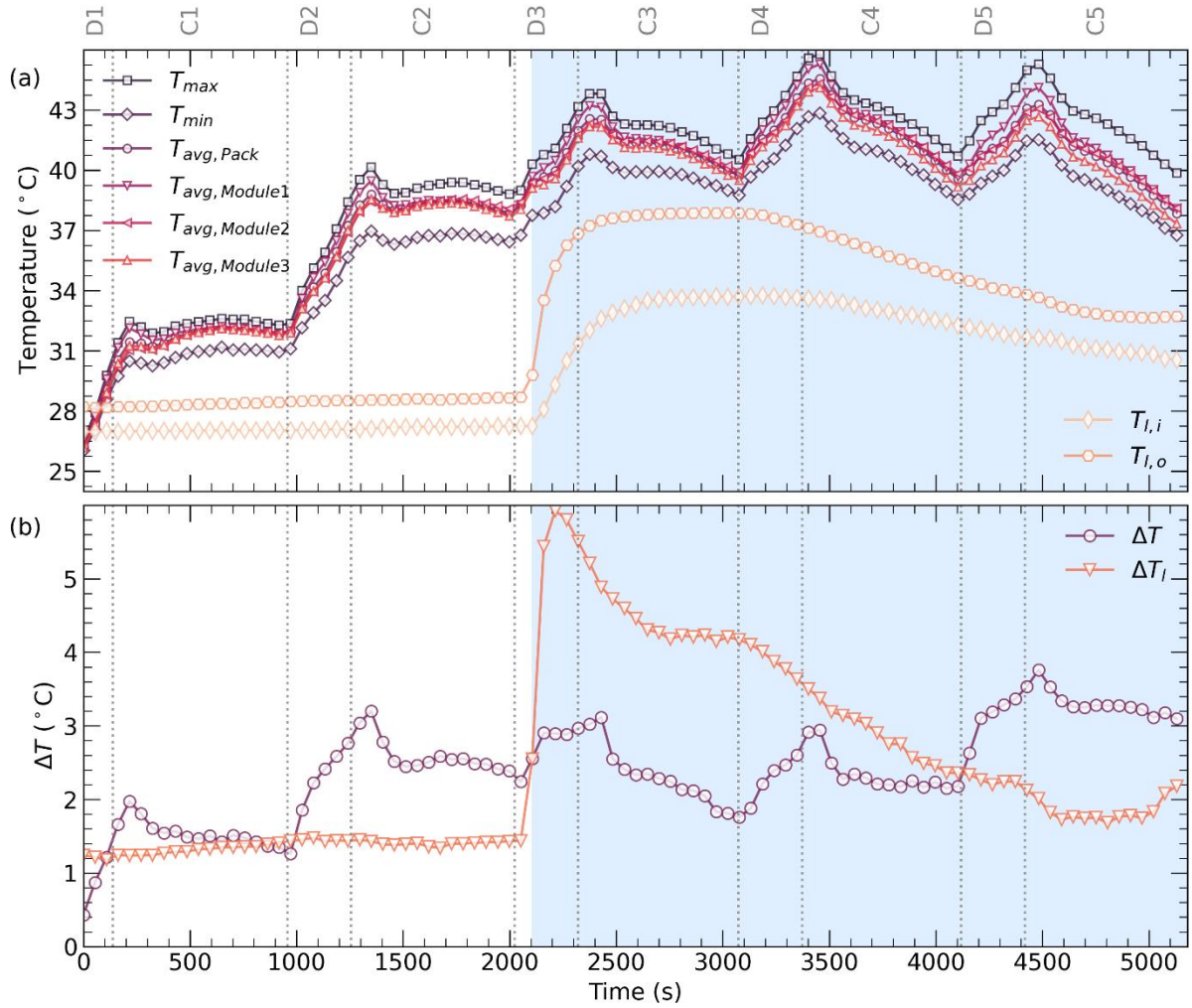

Figure 5. a) T_{avg}, T_{max}, and T_{min} of the pack and modules, as well as $T_{l,i}$ and $T_{l,o}$ of the liquid cooling system; b) ΔT behavior of the LIB pack and ΔT_l of the liquid cooling system. In both plots, the light blue area illustrates the active cooling portion of the test.

Furthermore, as the test progresses and enters into the active cooling portion, the maximum difference between T_{avg} of Module1 and the pack increases at each cycle (Figure 5a). In particular, the difference between T_{avg} of Module1 and the pack at the end of each high charging period in the passive cooling portion is approximately 0.6°C. Then, the difference increases and reaches a maximum difference of 0.9°C in the final cycle (C5) of the active cooling portion. This phenomenon illustrates the effect of the cooling system in amplifying the difference between the temperature behavior of each module and highlights the importance of conducting temperature distribution tests throughout the pack. Furthermore, it demonstrates that even within the same battery pack, different modules may exhibit varying temperature behaviors due to the cooling strategy. This underscores the need to optimize cooling strategies to minimize temperature differences.

3.2.3. Pack study

As shown in Figure 5a, the maximum temperature of the T_{avg} of the battery pack occurs during the charging periods (C1 to C5). Specifically, the maximum temperatures are observed at the beginning of the corresponding charging cycles, which is the position between the maximum charging current (237A)

and the remaining time. It is worth noting that during the low current charging periods of the passive cooling portion, the pack's temperature remains relatively constant. However, in the active cooling portion, the temperature decreases, resulting in a negative T_{rise}. The maximum decrease is observed in C5, where the temperature decreases by 5.4°C from the initial temperature of 42.9°C. This observation shows that during the low charge current period, the heat generated by the LIB pack is lower than the heat absorbed by the liquid medium, leading to a decrease in the pack's final temperature.

Examining Figure 5a, the T_{rise} during a full discharge in the passive cooling portion (D2) is approximately 5.8°C from the initial T_{avg} of the pack, which is 31.8°C. In the active cooling portion, the T_{rise} decreases to 4.2°C, 4.3°C, and 3.5°C for D3, D4, and D5, respectively, with initial T_{avg} values of 37.8°C, 39.8°C, and 39.4°C. Therefore, the liquid cooling system effectively reduces the T_{rise} compared to the passive cooling portion of the test.

Furthermore, the temperature rise in all discharge periods (Ds) follows a monotonic behavior, except for D3 (Figure 5a). This non-similarity can be attributed to the initial timing of the liquid cooling system activation, which occurs in the middle of D3. During this phase, there is an initial rise in $\Delta T_l(t)$ of the liquid cooling system, resulting in increased heat absorption from the battery pack (Figure 5b). This temporary change in the T_{rise} slope is influenced by the rise of $\Delta T_l(t)$. The maximum value of $\Delta T_l(t)$ is approximately 6.0°C and occurs shortly after the initial time of the active cooling portion (in 100s). $\Delta T_l(t)$ maintains this temperature for about 60s before gradually decreasing. At the minimum value, which occurs in C5, $\Delta T_l(t)$ reaches 1.7°C.

It is worth noting that the active cooling system starts at 2102s, coinciding with the $T_{max}(t)$, T_{avg}, and ΔT of the LIB pack reaching 40.2°C, 39.3°C, and 2.5°C, respectively (Figure 5a). $T_{l,i}(t)$ starts at the initial value of 27.2°C, reaches its maximum in the middle of C3 (37.9°C), and maintains this maximum temperature until the end of D4. Subsequently, its value gradually decreases, reaching 32.7°C by the end of the test. Similarly, $T_{l,o}(t)$ follows a similar pattern but with a higher temperature due to heat absorption during the test cycles.

In summary, in the LIB cells, modules, and pack, the temperature consistently rises during periods of high current (237A) such as the discharge cycles (Ds) and the beginning of each charging cycle (high current of Cs). Therefore, the over time T_{max} during each cycle occurs at the end of the constant charging portion of 237A (Equation 2). This temperature increase is attributed to a higher number of lithium-ions moving through the separator and producing more heat.

Furthermore, Figure 5b demonstrates the maximum ΔT values for each cycle, which occur in the middle of the charging sections (between the high charging current and the low charging current). The maximum ΔT values for the first to fifth cycles are 2.1°C, 3.3°C, 3.3°C, 3.1°C, and 3.9°C, respectively. These results indicate that the maximum ΔT of the pack remains below 4°C, which falls within the acceptable range for the temperature difference in a LIB pack [14,40–42]. The behavior of ΔT in the third cycle is similar to the temperature behavior and is influenced by the activation timing of the liquid cooling system (Figure 5b).

4. Conclusion

In conclusion, this study provides valuable insights into the thermal behavior of a 48V LIB pack under five dynamic charging-discharging current profiles. Understanding the thermal characteristics of LIB packs is essential for ensuring their safe and reliable operation, particularly in applications that demand high power and energy densities. This experimental study focused on a battery pack comprising three modules, each equipped with 12 prismatic LIB cells, and evaluated the impact of an indirect liquid cooling system on the pack's thermal behavior.

A homogeneous indirect liquid cooling system was applied to the bottom of the LIB modules once the pack temperature reached approximately 40.0°C (active cooling portion). Therefore, in the approximately first two cycles, the liquid did not flow through the cooling system (passive cooling portion). The temperature distribution of the battery pack and cooling system was measured and analyzed using 27 thermocouples. The high number of thermocouple utilization enabled a detailed

analysis of temperature behavior within the battery pack, facilitating a comprehensive evaluation of temperature distribution and identification of potential maximum temperature.

The results revealed the complex and nonlinear nature of the temperature behavior across different LIB cells, modules, and the entire pack, as well as the influence of the indirect liquid cooling system on the pack's thermal performance. Several key findings emerged from this study:

- The positive tab temperature was found higher than the negative tab temperature within a single cell, which is consistent with existing literature.
- One module exhibited higher sensitivity to high current, leading to a faster temperature rise and increased heat generation. This insight could only be obtained by studying all the modules within the same LIB pack.
- The temperature rises primarily resulted from high currents and the heat generated by moving lithium-ions through the separator.
- In the passive cooling portion, the external cells of the battery pack exhibited lower temperatures compared to the internal cells due to better convective heat transfer.
- The implementation of an indirect liquid cooling system (active cooling portion) altered the temperature distribution within the pack.
- The implementation of an indirect liquid cooling system demonstrated its effectiveness in controlling the maximum temperatures.
- The initial activation of the indirect liquid cooling system had a rapid impact on the LIB pack, driven by the high temperature difference between the inlet and outlet liquid temperatures.
- The liquid cooling system mitigated the temperature rise in high constant current conditions, enhancing the thermal performance of the LIB pack.
- The indirect liquid cooling system increased temperature differences within the pack. However, they remained within the safe range.

Future research could build upon these findings by investigating additional factors that may influence LIB thermal performance, such as different operating cycles, environmental conditions, and alternative cooling strategies. By considering these aspects, further advancements can be made toward optimizing the BTMSs of LIB packs and ensuring their reliable and safe operation in various applications.

Credit authorship contribution statement

The authors are listed in alphabetical order. A detailed description of each author's contribution to this work is provided in the following lines.

Antonio Paolo Carlucci: Conceptualization, Validation, Resources, Writing – review & editing, Supervision, Project administration. **Hossein Darvish**: Conceptualization, Methodology, Software, Validation, Formal analysis, Investigation, Resources, Data curation, Writing – original draft, Writing – review & editing, Visualization, Project administration. **Domenico Laforgia**: Validation, Resources, Supervision, Project administration, Funding acquisition.

References

[1] Emadi A 2014 *Advanced electric drive vehicles* (CRC Press)

[2] Bloomberg N E F 2022 Electric vehicle outlook 2022 *Exec. Sum*

[3] Chan C C 2007 The state of the art of electric, hybrid, and fuel cell vehicles *Proc. IEEE* **95** 704–18

[4] Englisch A, Pfund T, Reitz D, Simon E and Kolb F 2017 Synthesis of various hybrid drive systems *Der Antrieb von morgen 2017: Hybride und elektrische Antriebssysteme 11. Internationale MTZ-Fachtagung Zukunftsantriebe* (Springer) pp 61–78

[5] Zhuang W, Li S, Zhang X, Kum D, Song Z, Yin G and Ju F 2020 A survey of powertrain configuration studies on hybrid electric vehicles *Appl. Energy* **262** 114553

[6] Lee S, Cherry J, Safoutin M, McDonald J and Olechiw M 2018 Modeling and validation of 48v mild hybrid lithium-ion battery pack *SAE Int. J. Altern. Powertrains* **7** 273–88

[7] Lee S, Cherry J, Safoutin M, Neam A, McDonald J and Newman K 2018 *Modeling and controls development of 48 V mild hybrid electric vehicles* (SAE Technical Paper)

[8] Akbarzadeh M, Jaguemont J, Kalogiannis T, Karimi D, He J, Jin L, Xie P, Van Mierlo J and Berecibar M 2021 A novel liquid cooling plate concept for thermal management of lithium-ion batteries in electric vehicles *Energy Convers. Manag.* **231**

[9] Waldmann T, Hogg B-I and Wohlfahrt-Mehrens M 2018 Li plating as unwanted side reaction in commercial Li-ion cells – A review *J. Power Sources* **384** 107–24

[10] Bukhari S M A S, Maqsood J, Baig M Q, Ashraf S and Khan T A 2015 Comparison of characteristics--lead acid, nickel based, lead crystal and lithium based batteries *2015 17th UKSim-AMSS International Conference on Modelling and Simulation (UKSim)* (IEEE) pp 444–50

[11] Bloomberg N E F 2020 Electric vehicle outlook 2020 *Exec. Sum*

[12] Bloomberg N E F 2022 EV Transition Threatened as Battery Prices Rise for First Time *Exec. Sum*

[13] Liu Y, Gene Liao Y and Lai M-C 2020 Lithium-ion polymer battery for 12-voltage applications: Experiment, modelling, and validation *Energies* **13**

[14] Hu M, Wang J, Fu C, Qin D and Xie S 2016 Study on cycle-life prediction model of lithium-ion battery for electric vehicles *Int. J. Electrochem. Sci.* **11** 577–89

[15] Liu T, Liu Y, Wang X, Kong X and Li G 2019 Cooling control of thermally-induced thermal runaway in 18,650 lithium ion battery with water mist *Energy Convers. Manag.* **199** 111969

[16] Liu T, Tao C and Wang X 2020 Cooling control effect of water mist on thermal runaway propagation in lithium ion battery modules *Appl. Energy* **267** 115087

[17] Kim J, Oh J and Lee H 2019 Review on battery thermal management system for electric vehicles *Appl. Therm. Eng.* **149** 192–212

[18] Wu W, Wang S, Wu W, Chen K, Hong S and Lai Y 2019 A critical review of battery thermal performance and liquid based battery thermal management *Energy Convers. Manag.* **182** 262–81

[19] Tete P R, Gupta M M and Joshi S S 2021 Developments in battery thermal management systems for electric vehicles: A technical review *J. Energy Storage* **35** 102255

[20] Lin C, Liu Y, Zhang J, Han L, Fan B, Luo Y and Wang F 2019 Thermal uniformity of pouch-type lithium ion batteries with NCM cathode materials under different operating conditions *SAE Tech. Pap.* **2019-April**

[21] Kumar R and Chavan S 2022 Thermal Investigation of Cylindrical Lithium-ion Batteries for Different Loading using Experimental and Numerical Techniques *J. Electrochem. Soc.* **169** 120504

[22] Hall J, Borman S, Hibberd B, Bassett M, Reader S and Berger M 2020 48 V high-power battery pack for mild-hybrid electric powertrains *SAE Int. J. Adv. Curr. Pract. Mobil.* **2** 1893–904

[23] Monika K, Chakraborty C, Roy S, Dinda S, Singh S A and Datta S P 2021 Parametric investigation to optimize the thermal management of pouch type lithium-ion batteries with mini-channel cold plates *Int. J. Heat Mass Transf.* **164** 120568

[24] Wang R, Liang Z, Souri M, Esfahani M N and Jabbari M 2022 Numerical analysis of lithium-ion battery thermal management system using phase change material assisted by liquid cooling method *Int. J. Heat Mass Transf.* **183** 122095

[25] Pushkar K, Napa N, Madichetty S, Agrawal M K and Tamma B 2022 *Thermal Analysis of Lithium Ion Battery Pack with Different Cooling Media* (SAE Technical Paper)

[26] Carlucci A P, Darvish H and Laforgia D 2023 Detailed Thermal Characterization on a 48V Lithium-Ion Battery Pack during Charge-Discharge Cycles *Powertrains, Energy & Lubricants* (Kyoto, Japan: SAE Technical Paper)

[27] Zeng J, Feng S, Lai C, Song J, Fu L, Chen H, Deng S and Gao T 2023 Prediction on thermal performance of refrigerant-based battery thermal management system for a HEV battery pack *Int. J. Heat Mass Transf.* **201**

[28] Chen Y, Kang Y, Zhao Y, Wang L, Liu J, Li Y, Liang Z, He X, Li X, Tavajohi N and Li B 2021 A review of lithium-ion battery safety concerns: The issues, strategies, and testing standards *J. Energy Chem.* **59** 83–99

[29] Jürgens J 2019 This is Why NCM is the Preferable Cathode Material for Li-ion Batteries *LG Chem Partn. PortalThe BLOG Eur. Httpslghomebatteryblog Euenthis--Why-Ncm---Prefer.-Cathode-Mater.--Li-Ion-Batter.*

[30] Hesse H C, Schimpe M, Kucevic D and Jossen A 2017 Lithium-Ion Battery Storage for the Grid—A Review of Stationary Battery Storage System Design Tailored for Applications in Modern Power Grids *Energies* **10**

[31] Carlucci A P, Darvish H and Laforgia D 2023 *Thermal Performance of a 48V Prismatic Lithium-Ion Battery Pack Under WLTC Driving Cycles with a Liquid Cooling System* (SAE Technical Paper)

[32] Lyu P, Liu X, Liu C and Rao Z 2023 Experimental and modeling investigation on thermal risk evaluation of tabs for pouch-type lithium-ion battery and the relevant heat rejection strategies *Int. J. Heat Mass Transf.* **202** 123770

[33] Chindamo D and Gadola M 2018 What is the most representative standard driving cycle to estimate diesel emissions of a light commercial vehicle? *IFAC-Pap.* **51** 73–8

[34] An Z, Jia L, Wei L and Yang C 2018 Numerical modeling and analysis of thermal behavior and Li+ transport characteristic in lithium-ion battery *Int. J. Heat Mass Transf.* **127** 1351–66

[35] Pelkmans L and Debal P 2006 Comparison of on-road emissions with emissions measured on chassis dynamometer test cycles *Transp. Res. Part Transp. Environ.* **11** 233–41

[36] Tutuianu M, Bonnel P, Ciuffo B, Haniu T, Ichikawa N, Marotta A, Pavlovic J and Steven H 2015 Development of the World-wide harmonized Light duty Test Cycle (WLTC) and a possible pathway for its introduction in the European legislation *Transp. Res. Part Transp. Environ.* **40** 61–75

[37] Choi D, Wang D, Viswanathan V V, Bae I-T, Wang W, Nie Z, Zhang J-G, Graff G L, Liu J, Yang Z and Duong T 2010 Li-ion batteries from LiFePO4 cathode and anatase/graphene composite anode for stationary energy storage *Electrochem. Commun.* **12** 378–81

[38] Bao R, Avila V and Baxter J 2017 *Effect of 48 V mild hybrid system layout on powertrain system efficiency and its potential of fuel economy improvement* (SAE Technical Paper)

[39] Laidler K J 1984 The development of the Arrhenius equation *J. Chem. Educ.* **61** 494

[40] Kizilel R, Sabbah R, Selman J R and Al-Hallaj S 2009 An alternative cooling system to enhance the safety of Li-ion battery packs *J. Power Sources* **194** 1105–12

[41] Liu W, Jia Z, Luo Y, Xie W and Deng T 2019 Experimental investigation on thermal management of cylindrical Li-ion battery pack based on vapor chamber combined with fin structure *Appl. Therm. Eng.* **162** 114272

[42] Pesaran A A 2002 Battery thermal models for hybrid vehicle simulations *J. Power Sources* **110** 377–82

Definitions/Abbreviations

BMS	battery management system
BTMS	battery thermal management system
$\boldsymbol{CO_2}$	carbon dioxide
EV	electric vehicle
HEV	hybrid electric vehicle
LIB	lithium-ion battery
MHEV	mild hybrid electric vehicle
NCM	lithium nickel manganese cobalt oxide
SOC	state of charge

Contact Information

Antonio Paolo Carlucci is an associate professor in the Department of Engineering for Innovation at the University of Salento, Lecce, Italy. He is currently the director of "Engines, Combustion and Spray" lab. where research activities on combustion using liquid and gaseous alternative and renewable fuels in dual-fuel compression ignition and spark ignition engines are carried out. He has been involved in national and international projects on renewable fuels exploitation, energy recovery and energy production integrated systems. He coauthored numerous journal and conference papers and four book chapters.
✉ paolo.carlucci@unisalento.it

Hossein Darvish is a Ph.D. candidate in the Department of Engineering for Innovation at the University of Salento, Lecce, Italy. His research focuses on Thermal-Fluid Transport projects with applications to Lithium-Ion Battery Thermal Management Systems and Thermal Energy Storage, as well as Cardiovascular Biomechanics. Currently, he is completing his Ph.D. thesis at the Center for Studies of Vehicle Components in Bosch plant in Modugno, Bari, Italy, where he is involved in analyzing 48V lithium-ion battery packs and developing innovative climate chamber test benches to optimize their thermal management.
✉ hossein.darvish@unisalento.it

Domenico Laforgia is an Emeritus Professor in Energy Systems and Fluid Machinery and Scientific Coordinator of CREA research group at the University of Salento, Lecce, Italy. He coordinated as Scientific Responsible of many national and international projects on energy efficiency, renewable fuels exploitation, energy recovery, and energy production integrated systems. He has published over 350 international scientific articles and 17 books as well as seven patents in the field of energy efficiency.
✉ domenico.laforgia@unisalento.it